Competition between α and β decays for heavy deformed neutron-deficient Pa, U, Np, and Pu isotopes

Dongdong Ni[1,*] and Zhongzhou Ren[2,3,†]

[1]*Space Science Institute, Macao University of Science and Technology, Macao, China*

[2]*Department of Physics and Key Laboratory of Modern Acoustics, Institute of Acoustics, Nanjing University, Nanjing 210093, China*

[3]*Center of Theoretical Nuclear Physics, National Laboratory of Heavy-Ion Accelerator, Lanzhou 730000, China*

(Received 15 August 2016; revised manuscript received 13 October 2016; published 23 January 2017)

The competition between α and β decays is investigated for neutron-deficient Pa, U, Np, and Pu isotopes. β^+/electron-capture (EC) decay rates are calculated within the deformed quasiparticle random-phase approximation with realistic nucleon-nucleon (NN) interactions. Contributions from allowed Gamow-Teller and Fermi transitions as well as first-forbidden transitions are considered. α-decay calculations are performed within the generalized density-dependent cluster model. Effects of differences between neutron and proton distributions and nuclear deformation are taken into account. In the calculations, Reid-93 NN interactions are used for β^+/EC decays, while Michigan three-range Yukawa effective interactions, based on the G-matrix elements of Reid NN potentials, are used for α decay. The calculated β-decay half-lives show good agreement with the experimental data over a range of magnitude from 10^2 to 10^5 s. The resulting total half-lives including α and β contributions are found to be in good agreement with the experimental data, together with the α/β-decay branching ratios.

DOI: 10.1103/PhysRevC.95.014323

I. INTRODUCTION

The exploration for the limits of nuclear stability is one of the hot topics in current nuclear physics research. There is a worldwide effort to synthesize and investigate nuclei at the extremes such as high isospins and superheavy masses [1–6]. For exotic nuclei far from the stability line, most nuclear ground states are unstable against β decay to approach the stability line, either β^- decay for neutron-rich isotopes or β^+ and electron-capture (EC) decay for neutron-deficient isotopes. Near the drip lines they could even decay by nucleon emission to reduce their extremely high isospins. As for heavier elements, the nuclei are also unstable against α decay or spontaneous fission. In searching for the nuclear limits, the first thing one learns about a newly synthesized nucleus is its radioactive decay. The radioactive decay is usually the first tool to identify new nuclides and elements and hence also the first means to know its structure properties. Coincident observations of β and γ spectra have been used as powerful spectroscopic tools for exotic nuclei [7,8]. Very recently EC decay of ^{229}U has been investigated by γ-γ coincidence data and conversion electron measurements and a detailed level scheme in ^{229}Pa has been achieved [8]. In the heavy and superheavy mass region, new neutron-deficient isotopes have been populated by α decay and identified by observing α-decay events [9–12]. Very recently neutron-deficient U isotopes ^{216,221,222}U have been produced as evaporation residues in fusion reactions where α-α correlations or α-decay chains are used to identify new isotopes and isomers [11,12].

There is a competition between β^+/EC and α decays in the radioactive decay of neutron-deficient isotopes of actinide elements [13,14]. Their decay spectrums afford an excellent opportunity to investigate the structure properties of deformed heavy nuclei. Even a rough measurement of their half-lives and individual decay energies can provide important information on the proton-rich limit of stability for heavy nuclei. However, experimental decay data are rare for these neutron-deficient isotopes due to low statistics, especially for β^+/EC decay. In this work, we intend to investigate the β^+/EC and α decays of neutron-deficient Pa, U, Np, and Pu isotopes. The calculation of β^+/EC-decay rates is based on the deformed quasiparticle random phase approximation (QRPA) with realistic nucleon-nucleon (NN) interactions in large single-particle bases [15–17]. It is expected that more intruder single-particle states emerging in deformed heavy nuclei would enhance contributions from first-forbidden (FF) transitions [18,19]. So FF transitions are consistently considered within the deformed QRPA framework. The first attempt to include FF contributions was made within the statistical gross theory [20]. Later, Möller *et al.* computed allowed Gamow-Teller (GT) transitions within the deformed QRPA with separable GT residual interactions and estimated the average properties of FF decay by the gross theory for nuclear β^- decay [21,22]. In the past decade, microscopic QRPA treatments of FF transitions were also made to study the β^- decay of r-process waiting-point nuclei [15,23,24]. On the contrast, microscopic calculations of FF transitions are rare for nuclear β^+/EC decay, in particular for heavy nuclei, because β^+ and EC decays require different considerations and formulas of FF contributions [16,25]. Besides, various QRPA calculations of β decay have been shown to be successful for short-lived isotopes far from stability [26–34], but the QRPA results for long-lived isotopes are much less documented. In this context, another challenge in the present QRPA calculations is to reproduce the β^+/EC-decay half-lives of long-lived isotopes, since the neutron-deficient $Z = 91$–94 isotopes under investigation exhibit β-decay half-lives longer than 100 s in most cases. α-decay calculations are performed within the generalized

*dongdongnick@gmail.com

†zren@nju.edu.cn

density-dependent cluster model (GDDCM) [35–37]. The α-core potential is constructed in the double-folding model with effective NN interactions using the neutron and proton density distributions of daughter nuclei [35–38], and the effects of nuclear deformation and neutron skin thickness are taken into account [36,37]. The aim of the investigation is to describe the competition between β^+/EC and α decays precisely. Michigan three-range Yukawa (M3Y) effective interactions are used in the double-folding model for α-decay calculations. In order to gain more consistency, realistic Reid-93 NN interactions are used in the Brückner G matrix for β-decay calculations instead of the previously used charge-dependent Bonn (CD-Bonn) NN interaction.

This article is organized in the following way. In Sec. II, the deformed QRPA with realistic NN interactions is explained for β^+/EC decay and the GDDCM is presented for α decay. In Sec. III, the practical aspects of α- and β-decay calculations are discussed in detail. In Sec. IV, calculations are separately performed for β^+/EC and α decay and their competition is discussed and compared with the experimental data. A summary is given in Sec. V.

II. THEORETICAL FRAMEWORK

A. Deformed QRPA with realistic NN interactions for weak-decay calculations

The decay rates (in s^{-1}) for the weak process transforming a proton into a neutron are given by

$$\lambda = \frac{\ln 2}{K} \sum_f \lambda_{if}, \tag{1}$$

where the sum in f runs over daughter states within the Q_β window (i.e., $E_{\rm ex} < Q_\beta$) and the constant K is defined as $K = 2\pi^3\hbar^7 \ln 2/m_e^5c^4 = 6170$ s. For $\beta^\pm$ decay, the quantity λ_{if} is expressed in the form of the phase space integral [15,16,18,19,39],

$$\lambda_{if} = \int_1^{W_0} dW C(W) F(Z,R,W)(W_0 - W)^2 W\sqrt{W^2-1}, \tag{2}$$

where W_0 and W are the maximum energy and the total energy (including the rest energy) of the β particle in units of m_ec^2, Z and R are separately the atomic number and the nuclear radius of the daughter nucleus, $C(W)$ is the so-called shape factor depending on nuclear transition matrix elements, and $F(Z,R,W)$ is the Fermi function which accounts for the Coulomb distortion of the electron wave function near the daughter nucleus. The β maximum energy W_0 for β^+ decay is given by $W_0 = (Q_\beta - E_{\rm ex})/m_ec^2 - 1$, where $E_{\rm ex}$ is the excitation energy of the final state with respect to the ground state of the daughter nucleus. For EC decay, the quantity λ_{if} is expressed in the sum form [16,25],

$$f = \sum_x n_x C_x f_x^\epsilon, \tag{3}$$

where the sum in x runs over all electron subshells from which an electron can be captured, n_x is the fractional occupation number of the electron in the subshell x, and C_x and f_x^ϵ are, respectively, the shape factor and the phase space factor for the subshell x.

First, allowed Fermi and GT transitions are taken into account. Their shape factors are not dependent on the β energy W or the electron subsehll x and have the form

$$C(W) = B_{GT} = \left(\frac{g_A}{g_V}\right)^2_{\rm eff} \frac{|\langle f\|\vec{\sigma}\vec{\tau}_\pm\|i\rangle|^2}{2J_i+1}, \tag{4a}$$

$$C(W) = B_F = \frac{|\langle f\|\vec{\tau}_\pm\|i\rangle|^2}{2J_i+1}, \tag{4b}$$

where $(g_A/g_V)_{\rm eff}$ is the effective ratio of axial and vector coupling constants owing to the quenching of the GT strength. Then, contributions from FF transitions are considered. In the case of β^+ decay, the shape factor of FF transitions depends on the β energy W. If only dominant terms are considered, it can be written as [15,16,18,19]

$$C(W) = k(1 + aW + b/W + cW^2), \tag{5}$$

where k, ka, kb, and kc are the nuclear matrix elements associated with nuclear structure and their detailed expressions are given in Refs. [15,16,18,19]. In the case of EC decay, the shape factor of FF transitions is associated with the electron subshell. The shape factor for the subshell x (i.e., K, L_I, L_{II}, M_I, M_{II}, ...) can be expressed in terms of tensorial rank [16,25],

$$C_x = C_x^{(0)} + C_x^{(1)} + C_x^{(2)}. \tag{6}$$

The detailed expressions for $C_x^{(0,1,2)}$ can be found in Refs. [16,25].

On top of axially symmetric deformed mean-field calculations, the deformed proton-neutron QRPA with realistic NN interactions is employed to calculate the shape factors for allowed Fermi and GT transitions as well as for FF transitions. Here, we adopt an intrinsic coordinate frame for deformed calculations. In this frame, the projection K of the angular momentum on the symmetric axis and the parity π are good quantum numbers. The quasiparticle picture is constructed by the BCS treatment of nuclear pairing correlations and the QRPA phonon excitation operator is defined with the quasiparticle operators as

$$Q^\dagger_{m,K^\pi} = \sum_{pn} \left[X^m_{pn,K^\pi}\alpha^\dagger_p\alpha^\dagger_{\bar{n}} - Y^m_{pn,K^\pi}a_{\bar{p}}a_n\right], \tag{7}$$

where the sum in (pn) runs over the quasiparticle pairs $p\bar{n}$ with $\Omega_p - \Omega_n = K$ and $\pi_p\pi_n = \pi$, $\alpha^\dagger_\tau$ (α_τ) are quasiparticle creation (annihilation) operators, and $\alpha^\dagger_{\bar{\tau}}$ $(\alpha_{\bar{\tau}})$ are the time-reversed operators of $\alpha^\dagger_\tau$ (α_τ). The coefficients X^m_{pn,K^π} and Y^m_{pn,K^π} are, respectively, the forward and backward-going amplitudes of the mth QRPA phonon characterized by projection-spin K^π and energy $\omega^m_{K^\pi}$. They can be derived by solving the QRPA equations, where the two-body interaction matrix elements in the deformed single-particle basis are evaluated based on the Brückner G matrix with Reid-93 NN interactions. The details for the deformed interaction matrix elements are given in Refs. [15,16,40]. Here the Reid-93 NN interaction is employed in the Brückner G matrix calculation instead of the CD-Bonn interaction, as mentioned in the introduction. The

Reid-93 potential [41], as an updated regularized version of the Reid soft-core potential, consists of the one-pion-exchange (OPE) and non-OPE parts. The neutral-pion and charged-pion exchanges are distinguished in the OPE part, and the non-OPE part contains 50 phenomenological potential parameters A_{ip} and B_{ip} (the index i labels the different partial waves and p is an integer) which were determined to fit the NN scattering data available [41].

In the case of even-even nuclei, one can treat the ground state of parent nuclei as the BCS vacuum $|\tilde{0}\rangle_i = |QRPA\rangle \approx |BCS\rangle$ and the final states in the neighboring odd-odd nuclei as the QRPA phonon excited states $|m\rangle_f = Q^\dagger_{m,K^\pi}|QRPA\rangle$. The amplitude for β^+/EC transitions from $|\tilde{0}\rangle_i$ to the mth phonon state $|m\rangle_f$ is then expressed in the intrinsic frame by [15,16]

$$\langle mK^\pi|\beta^+_{JK}|\tilde{0}\rangle = \sum_{pn}\langle p|T_{JK}|n\rangle\left[v_p u_n X^m_{pn,K^\pi} + u_p v_n Y^m_{pn,K^\pi}\right]. \tag{8}$$

The one-body operators T_{JK} for FF transitions are connected with the following operators: $[\vec{r}\times\vec{\sigma}]^\lambda$ with $\lambda = 0, 1, 2$, and $\vec{r}$, as well as relativistic vector operator $\vec{\alpha}$ and axial charge operator γ_5 (for detailed forms, see Refs. [15,16]). Note that the absolute calculation of β-decay rates requires the excitation energy of the final state $E_{\rm ex}$ with respect to the ground state of the daughter nucleus. But the resulting QRPA energies ω_{K^π} are referred to the ground state of the parent nucleus and thus cannot be directly used. For even-even systems, the excitation energy $E_{\rm ex}$ of the final state can be obtained by subtracting a reference energy E_0 from the QRPA energy $\omega^m_{K^\pi}$ [30], i.e., $E_{\rm ex} = \omega^m_{K^\pi} - \omega_0$, where ω_0 represents the ground-state energy of the odd-odd daughter nucleus. Here the ω_0 value is determined as the lowest QRPA energy eigenvalue by solving the QRPA matrix equations with various K^π [15,16,23,24].

The case of odd-mass nuclei is more complicated. The ground state of parent nuclei is described as one quasiparticle state $|\tau\rangle_i = \alpha^\dagger_{\tau_i}|0\rangle$, where the unpaired nucleon occupies the single-particle orbital of the lowest energy. There are two types of β transitions available. One is a phonon excitation where the odd nucleon acts only as a spectator, named $\Delta\nu = 2$ transitions [42]. In this case, the intrinsic transition amplitude is essentially the same as the even-even case, but the blocked spectator is excluded from the sums in Eqs. (7) and (8). The other is a transition between one quasiparticle states in which the unpaired odd nucleon is involved, named $\Delta\nu = 0$ transitions [42]. In view of the coupling between the single quasiparticle and the QRPA phonon, phonon correlations to one-quasiparticle states are introduced in first-order perturbation theory. The explicit expression for the transition amplitude can be found in Ref. [43]. In this work, the allowed transition amplitude for the phonon-correlated one-quasiparticle state is exactly calculated in terms of the formalism presented in Ref. [43]. But for FF decay, we consider only the one-quasiparticle transitions without phonon correlations for simplicity, since FF decay is a higher-order process. For odd-mass systems, the excitation energy $E_{\rm ex}$ of the final state is derived in a different manner for $\Delta\nu = 2$ and $\Delta\nu = 0$ transitions. We take the β^+/EC decays of odd-neutron nuclei, for example. For $\Delta\nu = 2$ transitions with the unpaired nucleon as a spectator, the excitation energy $E_{\rm ex}$ is given by $E_{\rm ex} = (\omega + E_{n,\rm spect}) - E_{p_0}$, where ω is the QRPA energy, $E_{n,\rm spect}$ is the quasiparticle energy of the odd neutron, and E_{p_0} is the lowest proton quasiparticle energy. The term $(\omega + E_{n,\rm spect})$ denotes the energy of the daughter configuration with respect to the ground state of the neighboring even-even nucleus $(Z, N-1)$, and E_{p_0} denotes the ground-state energy of the daughter nucleus with respect to the even-even nucleus $(Z, N-1)$. For $\Delta\nu = 0$ transitions with the unpaired neutron involved, the excitation energy $E_{\rm ex}$ is given by $E_{\rm ex} = E_p - E_{p_0}$, where E_p is the quasiparticle energy of the resulting odd proton [33,34,42]. In terms of these two different determinations of $E_{\rm ex}$, it is found that the $\Delta\nu = 0$ transitions are able to occur in the low-excitation-energy region typically below twice the neutron pairing gap while the $\Delta\nu = 2$ transitions only occur in the higher excitation energy region. This feature is particularly important for long-lived nuclei with small β-decay energies [17].

B. GDDCM for α-decay calculations

α decay is traditionally understood as a two-body phenomenon, a single α cluster interacting with a core nucleus via a microscopic potential. Within the GDDCM, the α-core potential is numerically constructed using the double folded integral of effective NN interactions plus proton-proton Coulomb interactions with the density distributions of α particles and daughter nuclei [35–37],

$$V_{NorC}(\mathbf{r}) = \lambda\int d\mathbf{r_1}d\mathbf{r_2}\rho_1(\mathbf{r_1})\upsilon(\mathbf{s} = |\mathbf{r} + \mathbf{r_2} - \mathbf{r_1}|)\rho_2(\mathbf{r_2}), \tag{9}$$

where λ is used to renormalize the nuclear potential to reproduce an equivalent local potential ($\lambda = 1$ for the Coulomb potential). $\upsilon(\mathbf{s})$ is the effective NN interaction between a constituent nucleon in the α particle and one in the core nucleus. The popular M3Y NN interaction, based on the G-matrix elements of the Reid potential, is used for the nuclear potential. $\rho_1(\mathbf{r_1})$ and $\rho_2(\mathbf{r_2})$ are the matter/charge density distributions of the α particle and the residual core nucleus, respectively. The neutron and proton density distributions of the α cluster are expected to exhibit spherical symmetry and have the same form. They are described by a standard Gaussian form that is obtained from electron scattering data, $\rho_1(r_1) = \rho_1^0\exp(-0.7024r_1^2)$, where ρ_1^0 is determined by integrating the density distribution equivalent to the nucleon number. For the residual core nucleus, its density distribution could deviate from spherical symmetry. An axially symmetric shape with quadrupole and hexadecapole deformations (β_2, β_4) is usually considered. Furthermore, the neutron and proton distributions of the core nucleus are not exactly the same on the nuclear surface. In this work, the neutron and proton distributions of core nuclei are assumed to be of the two-parameter Fermi (2pF) form,

$$\rho_2^\tau(\mathbf{r_2}) = \frac{\rho_0^\tau}{1 + \exp\left[\left(r_2 - \mathbf{R}^\tau_{1/2}\right)/a_\tau\right]}, \tag{10}$$

where $\tau = n$ or p, and the half-density radius $\mathbf{R}^\tau_{1/2}$ is related to the mass number and deformation of the nucleus,

$\mathbf{R}^{\tau}_{\mathbf{1/2}} = r_\tau A^{1/3}[1 + \beta_2 Y_{20}(\theta) + \beta_4 Y_{40}(\theta)]$. The rms neutron and proton radii of the core nucleus are then conveniently written as

$$R_\tau \equiv \langle r^2 \rangle^{1/2} = \left[\int \rho_2^\tau(\mathbf{r}) r^4 dr d\Omega \Big/ \int \rho_2^\tau(\mathbf{r}) r^2 dr d\Omega \right]^{1/2}. \tag{11}$$

Despite the same 2pF form, different sets of parameters, (r_n, a_n) and (r_p, a_p), are used to characterize their differences. Their differences are gauged by the neutron skin thickness Δr_{np}. There are two extreme cases, namely, neutron skin type and neutron halo type distributions [44,45]. The neutron skin type distribution is understood as $r_n > r_p$ and $a_n = a_p$, while the neutron halo type distribution is understood as $r_n = r_p$ and $a_n > a_p$ [44,45]. In the skin type case, the diffuseness parameters are fixed at $a_n = a_p = 0.54$ fm and the radius parameters r_n and r_p are separately determined in terms of the neutron and proton rms radii, where the rms proton radius R_p is taken from the experimental rms charge radii and the rms neutron radius R_n is obtained by the relationship $R_n = R_p + \Delta r_{np}$. In the halo type case, the diffuseness parameter is fixed at $a_p = 0.54$ fm, the radius r_p is determined in terms of the experimental rms charge radii for the proton distribution, and then the diffuseness parameter a_n for the neutron distribution is determined in terms of the rms neutron radius $R_n = R_p + \Delta r_{np}$.

In the spherical approximation, the Schrödinger equation for the α-daughter system is numerically integrated in the spherical double-folding potential with outgoing wave boundary conditions. The renormalized factor λ of the nuclear potential is adjusted to reproduce the experimental α-decay energy and the quantum features ($n\ell j$) of the α cluster [46]. After achieving the cluster wave function $u_{n\ell j}(r)$, one can calculate the decay width in terms of the distorted-wave approach [36,37],

$$\Gamma = \frac{4\mu}{\hbar^2 k} \left| \int_0^\infty F_\ell(kr) \left[V_N(r) + V_C(r) - V_C^p(r) \right] u_{n\ell j}(r) dr \right|^2, \tag{12}$$

where $k = \sqrt{2\mu Q_\alpha}/\hbar$, $F_\ell(kr)$ is the regular Coulomb function, and $V_C^p(r)$ is the pointlike Coulomb potential $V_C^p(r) = Z_1 Z_2 e^2/r$. In the axially deformed case, the α particle can be emitted in any direction of the space, resulting in anisotropic α emission from an ensemble of oriented nuclei. This could be simply evaluated by integrating the partial width along the orientation [47],

$$\Gamma = \int_0^{\pi/2} \Gamma(\theta) \sin\theta d\theta, \tag{13}$$

where θ is the angle between the symmetry axis of the core nucleus and the direction of the α-particle emission, and $\Gamma(\theta)$ is calculated as in the spherical case (12). Such a straightforward technique has been widely used to calculate not only α-decay half-lives but also sub-barrier fusion cross sections between a spherically deformed pair of nuclei [47]. Ultimately, one should multiply the decay width by the α-preformation factor P_α which measures the extent to which the α cluster is formed on the nuclear surface. As before, one can take the same preformation factor for certain kinds of α emitters (even-even, odd-mass, and odd-odd), keeping the number of free parameters used in the model to a minimum [35–37]. Then, α-decay half-lives are calculated by the relationship $T_{1/2} = \hbar \ln 2/(P_\alpha \Gamma)$.

III. CALCULATION DETAILS

In weak-decay calculations, the single-particle basis is obtained by solving the Schrödinger equation in the axially deformed Woods-Saxon potential with the universal parametrization [48]. The single-particle model space for protons and neutrons contains some resonant states with energies up to 8 MeV in addition to bound states. In practice, we include the neutron single-particle levels with energies from -15.0 to 8.0 MeV and the proton single-particle levels with energies from -10.0 to 8.0 MeV, corresponding to the three major harmonic oscillator shells around the Fermi level in the spherical limit. The quasiparticle energies E_τ and pairing amplitudes (v_τ,u_τ) for protons and neutrons are separately obtained by solving the BCS equations with constant pairing gaps. The empirical pairing gaps Δ_τ are extracted from the nucleon separation energies [49]. Then, different intrinsic excitations K^π are considered using the QRPA matrix equations. Both particle-particle (pp) and particle-hole (ph) interaction matrix elements are considered by the Brückner G matrix with Reid-93 NN interactions and they are renormalized by the strength parameters g_{ph} and g_{pp}. We use the same g_{ph} and g_{pp} for all components K^π. This makes the calculation straightforward and keeps the relative strength of different components. It is well known that the ph strength mainly determines the energy position of GT giant resonances (GTGRs) at a high excitation energy. An appropriate value of g_{ph} can be achieved by the measurements or systematics on the GTGR energy [26]. Here the g_{ph} strength is fixed at a value of approximately $g_{ph} = 1.20$ for the heavy nuclei under investigation. The pp strength affects the QRPA energy of low-lying states and the transition strength to these states, both of which have direct influence on weak-decay rates. The sensitivity of the calculated results to the g_{pp} strength has been analyzed in Refs. [15,17], and here we do not repeat it. Two points should be noted, which are of particular relevance to the present calculation. For the heavy nuclei of this study, their β-decay energies are not so large. So the quasiparticle $\Delta\nu = 0$ transitions generally prevail over the phonon $\Delta\nu = 2$ transitions in odd-mass systems, because they always appears in the low-lying tail of the strength distribution and exactly enter in the narrow Q_β window. As already shown in Ref. [17], the g_{pp} strength has direct influence on the $\Delta\nu = 2$ transitions but affects the $\Delta\nu = 0$ transitions only through the weak phonon correlations emerging in first-order perturbation. Consequently, the calculated half-lives show weak dependence upon the g_{pp} strength for the odd-mass nuclei. Besides, it is known that larger g_{pp} strengths bring in smaller QRPA energies ω_{K^π}. The excitation energy $E_{\rm ex}$ of final states is taken as the difference between the QRPA energies in the case of even-even nuclei, as demonstrated above. This could reduce the effect of the g_{pp} strength on the excitation energy of final states to some extent. With these in mind, the g_{pp} strength is

fixed at $g_{pp} = 1.0$ in our calculations instead of a least-squares fit to the experimental half-lives.

Another important quantity is the quenching of the QRPA calculations for heavy nuclei. For the case of 0^- FF transitions, the tensor part of 0^- FF transitions seems to be enhanced due to meson exchange current effects. So the enhancement factor $\epsilon = g_A/g_A^{\rm free} = 2.0$ is usually adopted for the tensor part while the factor ϵ is fixed at 1.0 for the scalar part, as shown in Refs. [15–19,23,24]. Except for the 0^- FF case, the quenching effect is considered by using the effective ratio $(g_A/g_V)_{\rm eff} = q(g_A/g_V)_{\rm free}$ for both GT and FF transitions [50,51]. To determine the quenching factor q, it is assumed that the quenching factor is the same for GT and FF transitions. Here its value is determined by comparing the calculated half-lives with the experimental data. A choice of $q = 0.325$ turns out to well reproduce the β-decay half-lives. It should be pointed out that the experimental data would be better reproduced if the quenching factor is regarded to vary with the different transition operators as shown in Ref. [19]. Unfortunately, this procedure is not allowed at present, because there is little information available concerning the β^+/EC decay spectrum of heavy nuclei with $A \simeq 230$. Note that the q value presented here is smaller than some other pnQRPA calculations such as the relativistic pnQRPA built on the relativistic Hartree-Bogoliubov (RHB) model with $q = 0.79$ [52], the density function plus continuum QRPA model with $q = 0.90$ [53,54], and some pnQRPA calculations based on realistic NN interactions with $q = 0.40$–0.63 [24,50,51]. Very recently Deppisch and Suhonen have performed a statistical analysis of the effective axial-vector coupling constant g_A in the pnQRPA with Bonn-A interactions for the isobaric chains with $A = 62$–142 [55]. A considerable quenching of g_A is confirmed, as shown in Refs. [50,51]. Marketin *et al.* have performed a large-scale calculation of β-decay rates for neutron-rich nuclei with $8 \leqslant Z \leqslant 110$ within the RHB plus relativistic pnQRPA model [52], where the quenching of $q = 0.79$ is used for both GT and FF transitions of all nuclei. It is seen that their calculations predict shorter decay half-lives in the heavier mass region with $N > 126$ and $Z \sim 82$, suggesting a smaller quenching factor for these heavy nuclei. This also gives an active response to the quenching factor adopted in the present calculations. In addition, we would like to point out that the authors of Refs. [56,57] have taken more complicated configurations into account on top of self-consistent calculations with Skyrme density functionals, such as the coupling between one- and two-phonon configurations [56] and the particle-vibration coupling [57]. It is demonstrated that the low-lying GT strength is shifted downwards and becomes fragmented, leading to a clear decrease of the calculated β-decay half-lives for neutron-rich magic nuclei. Including more complicated states is supposed to improve β-decay calculations, but it requires suitable treatment of various couplings and large configuration spaces, in particular for deformed systems. This is an interesting issue and worthy of further investigation.

In α-decay calculations, the experimental rms charge radii are used to obtain the double-folding potentials when available; otherwise the simple relationship deduced from systematics of the experimental data is adopted [58], which is given by $R = (r_0 + r_1 A^{-2/3} + r_2 A^{-4/3})A^{1/3}$ with $r_0 = 0.891(2)$, $r_1 = 1.52(3)$, and $r_2 = -2.8(1)$ fm. Considering that the experimental Δr_{np} data are rare with large statistical error bars, following Refs. [36,37], the linear relationship between Δr_{np} and the asymmetry $\delta = (N - Z)/A$ is used for all heavy nuclei, which is expressed as $\Delta r_{np} = [-0.03(2) + 0.90(15)\delta]$ fm [45]. Moreover, in order to avoid introducing additional adjustable parameters into the present calculation, the P_α values are fixed in terms of the previous systematic calculations [36,37], that is, $P_\alpha \sim 0.078$ for even-even nuclei and $P_\alpha \sim 0.051$ for odd-mass nuclei.

TABLE I. Effects of the single-particle spectra on β-decay results for some Pu isotopes. The experimental spin parities and β-decay half-lives are taken from Ref. [14]. Calculations are separately performed with the two different level schemes: the universal and optimal parametrizations of the Woods-Saxon potential.

Nucl.	Expt.		Universal		Optimal	
	J^π	$T_{1/2,\beta}$ (s)	J^π	$T_{1/2,\beta}$ (s)	J^π	$T_{1/2,\beta}$ (s)
^{231}Pu	$3/2^+$[a]	593	$3/2^+$	393	$5/2^-$	660
^{232}Pu	0^+	2.25×10^3	0^+	393	0^+	390
^{233}Pu	$5/2^+$[a]	1.26×10^3	$5/2^-$	1.59×10^3	$3/2^+$	812
^{234}Pu	0^+	3.37×10^4	0^+	5.77×10^3	0^+	5.17×10^3
^{235}Pu	$5/2^+$	1.52×10^3	$5/2^+$	4.50×10^3	$5/2^+$	4.85×10^3

[a]Values estimated from trends in neighboring nuclides.

As is always the case, the calculation of the present type depends to some extent on the single-particle spectrum adopted. For α decay, the single-particle level schemes just affect the α clustering of four valence nucleons at the nuclear surface. It has been shown that the α-preformation factors vary smoothly in the open-shell region for heavy nuclei [59,60]. So α-decay rates are significantly determined by the dynamic properties of α clusters (i.e., the barrier penetration probability) rather than the single-particle properties. By contrast, β-decay properties are closely associated with nuclear structure and have more dependence upon the single-particle level schemes. Here the deformed single-particle basis is achieved with an axially deformed Woods-Saxon potential for β^+/EC decays. To discern such an unfortunate dependence, β-decay calculations are performed with two different single-particle level schemes corresponding to the universal and optimal Woods-Saxon parametrizations [48]. The significant difference between the universal and optimal parametrizations lies in the spin-orbit potential: the strength λ and radius r_{0-so} parameters separately show characteristic oscillations as function of the nucleon number for protons and neutrons in the optimal case, while they are fixed as $\lambda_p = 36$, $\lambda_n = 35$, $r^p_{0-so} = 1.20$ fm, and $r^n_{0-so} = 1.31$ fm in the universal case. The details can be found in Ref. [48]. Table I displays the numerical results for some Pu isotopes. As can be seen, there are minor changes in the β-decay half-lives calculated with the different level schemes for the even-even Pu isotopes. But for ^{231,233}Pu, the single-particle levels occupied by the last unpaired neutron are different in the two cases and the differences of the results are relatively apparent within a factor of roughly 2. This is attributed to the additional $\Delta\nu = 0$ transitions in odd-mass

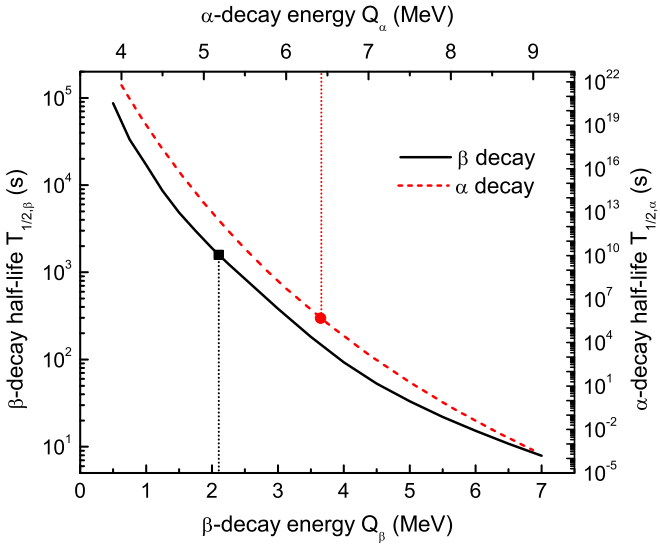

FIG. 1. Sensitivity of the calculated half-life to the decay energy used in calculations for the β^+/EC and α decays of ^{233}Pu. The β^+/EC-decay results are shown by black solid lines (left axis: calculated β-decay half-life, bottom axis: β-decay energy), while the α-decay results are shown by red dashed lines (right axis: calculated α-decay half-life, top axis: α-decay energy). Also, the experimental β^+/EC-decay and α-decay energies are, respectively, indicated by black and red dotted lines.

systems which is directly correlated with the single-particle spectrum.

IV. RESULTS AND DISCUSSION

The β-decay energy Q_β determines the window in the low-lying tail of the β-strength distribution and has direct influence on the size of the phase space. Figure 1 shows the variation of the calculated half-life as a function of the Q_β value for the β^+/EC decay of ^{233}Pu. When one changes the Q_β value from 1.0 to 4.0 MeV, the calculated half-life is decreased by about two orders of magnitude from 10^4 to 10^2 s. Furthermore, the decrease of the calculated half-life becomes relatively smoother in the larger Q_β values. It is also of interest to gain insight into the theoretical uncertainty owing to the error bars of the Q_β values. For example, the error bar of $Q_\beta = 3610(100)$ keV for ^{229}Pu leads to an uncertainty of roughly $-14.5/+17.0\%$ in the calculated half-life $T_{1/2,\beta} = 2.27 \times 10^2$ s. For ^{232}Pu, the experimental Q_β value is still unknown and the value of 1000(100) keV deduced from the Q_β values of neighboring isotopes is used instead [49]. The resulting uncertainty of the calculated half-life $T_{1/2,\beta} = 3.93 \times 10^2$ s is evaluated as $-24.2/+34.7\%$. As one would expect, the same Q_β error bar results in larger uncertainties of the calculated half-lives for smaller Q_β values. It is well known that the α-decay half-life is significantly dependent upon its decay energy. The sensitivity of the calculated α-decay half-life to the decay energy is also illustrated in Fig. 1 for the α decay of ^{233}Pu. As the decay energy Q_α is varied from 5.0 to 8.0 MeV, the calculated half-life decreases sharply by about 14 orders of magnitude from 10^{13} to 10^{-1} s. Obviously, the

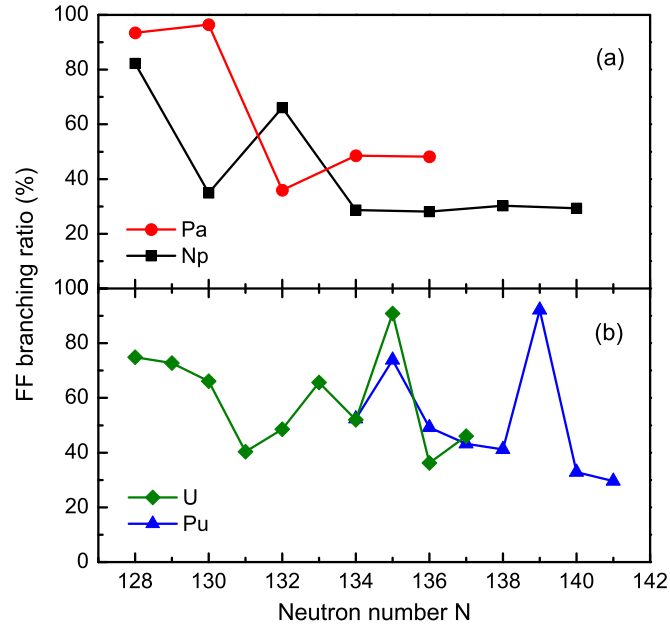

FIG. 2. Percentage of the contributions of FF transitions to the β^+/EC decay rates of the neutron-deficient Pa, U, Np, and Pu isotopes.

α-decay half-life is much more sensitive to the decay energy than the β-decay half-life. The error bar of experimental Q_α values is generally about 10 keV for the even-even isotopes, while the error bar of Q_α values is mostly more than 20 keV for the odd-mass isotopes. Specifically, the experimental Q_α value for ^{232}Pu is known as 6716(10) keV, yielding an uncertainty of about $-9.7/+10.3\%$ in the calculated α-decay half-life. For ^{233}Pu, the error bar of $Q_\alpha = 6420(50)$ keV leads to an effect of roughly $-41.5/+69.4\%$.

FF transitions proceed with the change of parity and their contributions to weak-decay rates are correlated with the appearance of intruder single-particle orbitals. In heavy nuclei, there are more intruder single-particle orbitals with different parities around the Fermi levels. Thus it is expected that FF transitions contribute to the weak-decay rate of heavy nuclei in addition to allowed GT and Fermi transitions. Let us discern the contribution of FF transitions to β-decay rates. The calculated branching ratios (BRs) of FF transitions are illustrated in Fig. 2 for the Pa, Np, U, and Pu isotopic chains. The variation of BRs with increasing neutron number shows some interesting features. In Fig. 2(a), the BRs exhibit large values for the onset Pa isotopes ^{219,221}Pa corresponding to the spherical region. Based on the spherical shell model, it can be easily understood since the valence neutrons and protons separately occupy two adjacent major shells with different parities. An accentuated decrease is then seen after $N = 130$. This may be attributed to the shape transition between spherical and deformed nuclei and/or the known deformed neutron subshell $N = 130$. For the Np isotopes, the moderately deformed isotope ^{221}Np exhibit similar BRs as the spherical Pa isotopes, the followed decrease can be associated with the shape transition from spherical to deformed systems, and then the obvious increase after $N = 130$ can be understood as the result of the deformed

TABLE II. Results for the neutron-deficient Pa, U, Np, and Pu isotopes where β^+/EC decay is in competition with α decay. The experimental data on β-decay energies, total half-lives, and β-decay branching ratios (BRs) are, respectively, shown in columns 2–4. Columns 5 and 6 give the β^+/EC decay half-lives deduced from the available data and the calculated values. Combined the β-decay results with the α-decay calculations, the theoretical results concerning β-decay BRs and total half-lives are also given in the last two columns.

Nucl.	Q_β (MeV)	$T_{1/2}^{\rm expt}$	$\rm BR_\beta$ (%)	$T_{1/2,\beta}^{\rm expt}$ (s)	$T_{1/2,\beta}^{\rm calc}$ (s)	$\rm BR_\beta^{calc}$ (%)	$T_{1/2}^{\rm calc}$
^{219}Pa	4.070(70)	53(10) ns	3×10^{-8}[a]	>100[a]	1.27×10^2	1.69×10^{-7}	215 ns
^{221}Pa	3.440(50)	5.9(17) μs	?	2.12×10^1[a]	2.35×10^2	7.45×10^{-6}	17.5 μs
^{223}Pa	2.930(70)	5.1(3) ms	?	5.67×10^1[a]	1.83×10^2	2.90×10^{-3}	5.30 ms
^{225}Pa	2.030(70)	1.7(2) s	?	>100[a]	8.01×10^2	0.60	4.78 s
^{227}Pa	1.026(7)	38.3(3) min	15(2)	1.53×10^4	4.63×10^3	53.8	41.49 min
^{220}U	2.720(110)[b]	60 ns[b]	?	5.75×10^1[a]	7.92×10^0	1.95×10^{-6}	155 ns
^{221}U	4.110(110)[b]	0.70 μs[b]	?	>100[a]	1.30×10^2	1.17×10^{-6}	1.52 μs
^{222}U	2.070(120)[b]	4.7(7) μs	?	1.12×10^1[a]	2.05×10^1	3.34×10^{-5}	6.8 μs
^{223}U	3.520(100)	55(10) μs	?	2.29×10^1[a]	9.23×10^1	2.64×10^{-4}	243 μs
^{224}U	1.851(26)	0.940(270) ms	?	>100[a]	3.62×10^1	2.98×10^{-3}	1.078 ms
^{225}U	3.040(70)	61(4) ms	?	>100[a]	3.02×10^2	3.35×10^{-2}	101 ms
^{226}U	1.296(17)	269(6) ms	?	>100[a]	1.72×10^2	0.384	660 ms
^{227}U	2.190(18)	1.1(1) min	<6[a]	>100[a]	1.14×10^3	3.8	0.72 min
^{228}U	0.298(15)	9.1(2) min	<5	$>1.09 \times 10^4$	1.34×10^4	7.6	17.03 min
^{229}U	1.313(7)	57.8(5) min	~80	4.34×10^3	2.47×10^3	95.6	39.42 min
^{221}Np	5.360(220)[b]	100 ns[b]	?	4.35×10^0[a]	2.49×10^1	9.98×10^{-7}	248 ns
^{223}Np	4.760(210)[b]	1 μs[b]	?	1.73×10^1[a]	1.94×10^1	5.15×10^{-5}	9.98 μs
^{225}Np	4.210(70)	3 ms[b]	?	9.63×10^0[a]	1.33×10^2	1.05×10^{-3}	1.4 ms
^{227}Np	3.540(70)	510(60) ms	?	2.47×10^1[a]	1.16×10^2	0.80	926 ms
^{229}Np	2.570(90)	4.00(18) min	32(11)	7.50×10^2	3.16×10^2	67.9	3.58 min
^{231}Np	1.820(50)	48.8(2) min	98(1)	2.99×10^3	8.48×10^2	99.7	14.10 min
^{233}Np	1.030(50)	36.2(1) min	~100	2.17×10^3	4.55×10^3	99.9997	75.91 min
^{228}Pu	2.480(60)	2.1(13) s	<7[a]	4.74×10^1[a]	1.79×10^1	3.1	0.56 s
^{229}Pu	3.610(100)	91(26) s	50(20)	1.82×10^2	2.27×10^2	5.1	11.52 s
^{230}Pu	1.700(50)	1.70(17) min	?	>100[a]	6.55×10^1	79.2	0.87 min
^{231}Pu	2.660(60)	8.6(5) min	87(5)	5.93×10^2	3.93×10^2	95.3	6.24 min
^{232}Pu	1000(100)[b]	33.7(5) min	90[a]	2.25×10^3	3.93×10^2	97.7	6.40 min
^{233}Pu	2.100(70)	20.9(4) min	99.88(5)	1.26×10^3	1.59×10^3	99.68	26.43 min
^{234}Pu	0.393(11)	8.8(1) h	~94	3.37×10^4	5.77×10^3	99.4	1.59 h
^{235}Pu	1.139(21)	25.3(5) min	99.9972(7)	1.52×10^3	4.50×10^3	99.9950	75.00 min

[a]Values are taken from the theoretical results of Möller *et al.* [21].
[b]Values are derived from trends in neighboring nuclei [14,49].

neutron subshell $N = 130$. One can also notice in Fig. 2(a) that the variations of the BRs seem to show the opposite behaviors for the Pa and Np isotopic chains. This may be a good indication of the known deformed proton subshell $Z = 92$. For the U isotopic chain in Fig. 2(b), the depression after $N = 130$ can be also correlated with the shape transition and/or the deformed neutron subshell $N = 130$, while the bulge after $N = 134$ can be an indication of the deformed neutron subshell $N = 134$ for $Z = 92$. In the Pu isotopic chain there is an evident bulge after $N = 138$, showing an indication of the deformed neutron subshell $N = 138$ for $Z = 94$. Additionally, the newly established EC-decay scheme of ^{229}U demonstrates that the FF contribution are comparable with the allowed contribution. The present calculation yields the FF BR of about 46.0% for the β decay of ^{229}U, giving an active response to the new data. On the whole, FF transitions have significant contributions to the β^+/EC decay rates of heavy nuclei and show good correlations with nuclear structure properties.

In the $A \simeq 230$ region, the β-decay BRs of many isotopes are not experimentally determined or they are measured with large error bars due to low statistics [13,14]. And hence their experimental β-decay half-lives are unknown or known with large uncertainties. In this case, some systematical calculations are referred as preliminary such as the finite-range droplet model plus QRPA [21]. The comparison of the calculated β^+/EC decay half-lives with the available data is displayed in Table II. The second column is the experimental Q_β value. The third and fourth columns are the experimental or deduced data on total half-lives and β-decay BRs. Columns 5 and 6 separately list the deduced β-decay half-lives and the calculated values. It is relevant to mention here that a precise calculation of the β-decay half-lives of long-lived nuclei is a formidably difficult task within the QRPA framework. Möller *et al.* regarded that their half-life calculations are successful in describing the β decay of short-lived nuclei far from stability but they may be not reliable for long-lived nuclei near the β-stability line; and hence only the theoretical results shorter than 100 s were compared with the experimental data in the tables [21,22]. Here, the known β-decay half-lives are generally longer than 100 s (up to 10^5 s), as shown in column 5

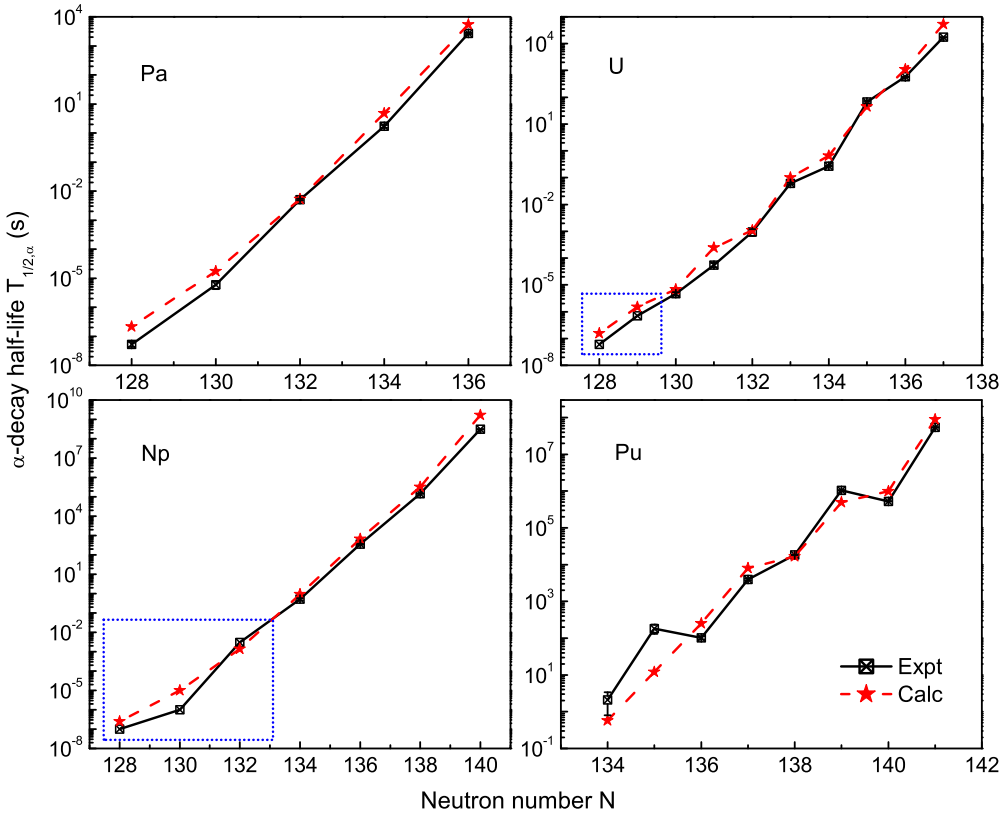

FIG. 3. Comparison of the calculated α-decay half-lives with the experimental values versus the neutron number N of parent nuclei for the α decays of the neutron-deficient Pa, U, Np, and Pu isotopes. α-decay calculations are performed with the neutron skin type distribution. Experimental α-decay data are not explicitly determined for some extremely neutron-deficient nuclei and deduced values suggested in Refs. [14,49] are illustrated instead. These cases are indicated by blue dotted squares and recognized by quite large uncertainties.

of Table II. However, one can see that the present calculations show good agreement with the available experimental data. The standard deviation for 11 isotopes is evaluated as $\sigma = 0.46$ corresponding to a factor of about 2.87. This is quite consistent with the previous β^+/EC decay calculation [16], where the β-decay half-lives of neutron-deficient Kr, Sr, Zr, and Mo isotopes are well reproduced within a factor of about 2.11 over a wide range of magnitude from 10^{-2} to 10^{7} s. Moreover, predictions of β-decay half-lives are made for some more neutron-deficient isotopes, which could be useful for future experiments.

The experimental α-decay data for the heavy nuclei are relatively full with respect to the β-decay data, since α decay serves as a powerful tool to populate and identify heavy neutron-deficient isotopes and half-lives of very neutron-deficient isotopes are mainly determined by α decay. It has been demonstrated in the previous α-decay studies [36,37] that the neutron skin-type and neutron halo type treatments of neutron skin thickness yield quite similar results concerning α-decay half-lives. So here we take the neutron skin type case for an example. Figure 3 shows the comparison of the calculated α-decay half-lives with the experimental data versus the neutron number of parent nuclei. For some extremely neutron-deficient U and Np isotopes, their α-decay measurements are unavailable in present facilities and the estimated values suggested in Refs. [14,49] are displayed instead. These cases are indicated by blue dotted squares and recognized by quite large uncertainties. First, indication of deformed neutron subshell closures are found from the available α-decay half-lives. There is an evident bump at $N = 134$ in the U isotopic chain, corresponding to the deformed neutron subshell closure. There is also a bump at $N = 130$ in the Np isotopic chain. Besides, the odd-even effect can be seen in the Pu isotopic chain except for $N = 138$. Such an abnormal case implies that the Pu isotope with $N = 138$ exhibits a smaller Q_α value than expected and hence $N = 138$ may be a deformed subshell closure for $Z = 94$. These are consistent with the results deduced from the above BRs analysis for FF transitions. Second, the calculated results follow the experimental data well over a wide range of magnitude from 10^{-8} to 10^{8} s. The largest deviation appears for the odd-mass isotope ^{229}Pu where the α-decay half-life is underestimated by about one order of magnitude. This can be explained if the α decay of ^{229}Pu is hindered with the angular momentum $\ell \neq 0$. Indeed, there exist some theoretical evidences for this [14], although the experimental α spectrum of ^{229}Pu is not available. If one treats the decay as unfavored α decays, the P_α factor as well as the barrier penetration probability would become smaller, leading to a clear increase in the half-life and hence better agreement with the experimental data.

To gain insight into the competition between β^+/EC and α decays, the above weak-decay and α-decay calculations

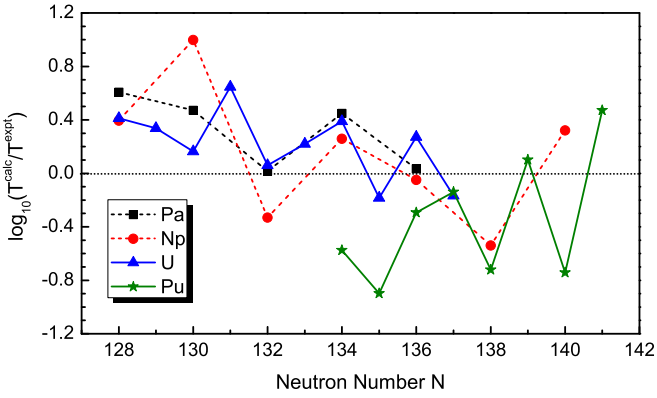

FIG. 4. Deviations of the calculated total half-lives (including β^+/EC and α contributions) from the experimental half-lives for the neutron-deficient Pa, U, Np, and Pu isotopes.

are combined to obtain the total decay half-lives as well as the BRs of individual decay modes. The calculated β-decay BRs and total half-lives are listed in the last two columns of Table II. Based on the β-decay BRs, one can see that α decay plays a crucial role in the radioactive decay of very neutron-deficient isotopes and contributions from β^+/EC decay become more considerable with increasing neutron number. Near the stability line, β^+/EC decay takes the place of α decay and dominates the radioactive decay of relatively long-lived isotopes. For the sake of clarity, we also display in Fig. 4 the deviations of the calculated total half-lives from the experimental data for the neutron-deficient Pa, U, Np, and Pu isotopes. Despite the deformations involved in both β and α decays, the theoretical total half-lives agree with the experimental ones well. The obvious derivations from the experimental data occur for ^{223}Np and ^{229}Pu, where their total half-lives are almost contributed by α decay. For ^{223}Np, both the experimental α-decay energy and half-life are still unknown and the estimated values with quite large uncertainties are used for reference. For ^{229}Pu, its α-decay from ground states to ground states could be hindered by a considerable hindrance to α-cluster formation together with an additional centrifugal barrier to penetration. As a result, the favored α-decay calculation yields an obvious underestimation of its α-decay half-life, as explained above.

V. SUMMARY

In summary, we have investigated in this paper the competition between α and β decays for deformed neutron-deficient Pa, U, Np, and Pu isotopes. β^+/EC decay rates are calculated within the deformed QRPA for even-even and odd-mass nuclei. The residual particle-particle and particle-hole interaction matrix elements in the deformed basis are determined based on the Brückner G matrix with Reid-93 NN forces. The contributions from both allowed (including GT and Fermi) and FF transitions are considered using the QRPA equations with different intrinsic excitations and the FF branching ratios are discussed. The generalized density-dependent cluster model (GDDCM) is employed to calculate α-decay half-lives. The α-core potential is constructed in the double-folding model with M3Y effective interactions based on the G matrix of Reid NN potential, and differences between neutron and proton distributions of daughter nuclei are taken into account. Both β^+/EC-decay and α-decay half-lives are computed and compared with the available experimental data. The resulting total half-lives contributed by β^+/EC and α decays are found to be in good agreement with the experimental data and the calculated β-decay branching ratios agree with the experimental data as well. Moreover, predictions of β-decay half-lives and branching ratios are made for some very neutron-deficient isotopes, where α decay plays a dominant role and β decay has not been observed or measured up to now.

ACKNOWLEDGMENTS

This work is supported by the Science and Technology Development Fund of Macau under Grants No. 007/2016/A1 and No. 039/2013/A2, by the National Natural Science Foundation of China (Grants No. 11535004, No. 11035001, No. 11165006, No. 10735010, and No. 10975072), by the 973 National Major State Basic Research and Development of China (Grants No. 2013CB834400 and No. 2010CB327803), and by the Project Funded by the Priority Academic Programme Development of JiangSu Higher Education Institutions (PAPD).

[1] S. Nishimura *et al.*, Phys. Rev. Lett. **106**, 052502 (2011).
[2] T. Kurtukian-Nieto *et al.*, Phys. Rev. C **89**, 024616 (2014).
[3] G. Lorusso *et al.*, Phys. Rev. Lett. **114**, 192501 (2015).
[4] S. Hofmann and G. Münzenberg, Rev. Mod. Phys. **72**, 733 (2000).
[5] P. A. Ellison *et al.*, Phys. Rev. Lett. **105**, 182701 (2010).
[6] Yu. Ts. Oganessian and V. K. Utyonkov, Nucl. Phys. A **944**, 62 (2015).
[7] B. Rubio, W. Gelletly, E. Nácher, A. Algora, J. L. Taín, A. Pérez, and L. Caballero, J. Phys. G: Nucl. Part. Phys. **31**, S1477 (2005).
[8] I. Ahmad, R. R. Chasman, J. P. Greene, F. G. Kondev, and S. Zhu, Phys. Rev. C **92**, 024313 (2015).
[9] C. A. Laue *et al.*, Phys. Rev. C **59**, 3086 (1999).
[10] K. Nishio, H. Ikezoe, S. Mitsuoka, K. Satou, and C. J. Lin, Phys. Rev. C **68**, 064305 (2003).
[11] J. Khuyagbaatar *et al.*, Phys. Rev. Lett. **115**, 242502 (2015).
[12] L. Ma *et al.*, Phys. Rev. C **91**, 051302(R) (2015).
[13] NNDC of the Brookhaven National Laboratory, http://www.nndc.bnl.gov/.
[14] G. Audi, F. G. Kondev, M. Wang, B. Pfeiffer, X. Sun, J. Blachot, and M. MacCormick, Chin. Phys. C **36**, 1157 (2012).
[15] D. Ni and Z. Ren, Phys. Rev. C **89**, 064320 (2014).
[16] D. Ni and Z. Ren, Phys. Lett. B **744**, 22 (2015).
[17] D. Ni and Z. Ren, Phys. Rev. C **92**, 034324 (2015).
[18] T. Suzuki, T. Yoshida, T. Kajino, and T. Otsuka, Phys. Rev. C **85**, 015802 (2012).

[19] Q. Zhi, E. Caurier, J. J. Cuenca-García, K. Langanke, G. Martínez-Pinedo, and K. Sieja, Phys. Rev. C **87**, 025803 (2013).
[20] K. Takahashi, M. Yamada, and T. Kondoh, At. Data Nucl. Data Tables **12**, 101 (1973).
[21] P. Möller, J. R. Nix, and K.-L. Kratz, At. Data Nucl. Data Tables **66**, 131 (1997).
[22] P. Möller, B. Pfeiffer, and K.-L. Kratz, Phys. Rev. C **67**, 055802 (2003).
[23] D.-L. Fang, B. A. Brown, and T. Suzuki, Phys. Rev. C **88**, 024314 (2013).
[24] D.-L. Fang, B. A. Brown, and T. Suzuki, Phys. Rev. C **88**, 034304 (2013).
[25] D. E. Alburger and E. K. Warburton, Phys. Rev. C **38**, 1843 (1988).
[26] J. Suhonen, T. Taigel, and A. Faessler, Nucl. Phys. A **486**, 91 (1988).
[27] J. Suhonen and O. Civitarese, Phys. Lett. B **280**, 191 (1992).
[28] H. Homma, E. Bender, M. Hirsch, K. Muto, H. V. Klapdor-Kleingrothaus, and T. Oda, Phys. Rev. C **54**, 2972 (1996).
[29] J. Engel, M. Bender, J. Dobaczewski, W. Nazarewicz, and R. Surman, Phys. Rev. C **60**, 014302 (1999).
[30] M. Martini, S. Péru, and S. Goriely, Phys. Rev. C **89**, 044306 (2014).
[31] T. Nikšić, T. Marketin, D. Vretenar, N. Paar, and P. Ring, Phys. Rev. C **71**, 014308 (2005).
[32] A. A. Raduta, C. M. Raduta, and A. Escuderos, Phys. Rev. C **71**, 024307 (2005).
[33] P. Sarriguren, A. Algora, and J. Pereira, Phys. Rev. C **89**, 034311 (2014).
[34] P. Sarriguren, Phys. Rev. C **91**, 044304 (2015).
[35] D. Ni and Z. Ren, Phys. Rev. C **80**, 051303(R) (2009); **81**, 024315 (2010).
[36] D. Ni and Z. Ren, Phys. Rev. C **92**, 054322 (2015).
[37] D. Ni and Z. Ren, Phys. Rev. C **93**, 054318 (2016).
[38] D. S. Delion, S. Peltonen, and J. Suhonen, Phys. Rev. C **73**, 014315 (2006).
[39] Y. Ren and Z. Ren, Phys. Rev. C **89**, 064603 (2014).
[40] M. S. Yousef, V. Rodin, A. Faessler, and F. Šimkovic, Phys. Rev. C **79**, 014314 (2009).
[41] V. G. J. Stoks, R. A. M. Klomp, C. P. F. Terheggen, and J. J. de Swart, Phys. Rev. C **49**, 2950 (1994).
[42] P. Möller and J. Randrup, Nucl. Phys. A **514**, 1 (1990).
[43] K. Muto, E. Bender, and H. V. Klapdor, Z. Phys. A **333**, 125 (1989).
[44] A. Trzcińska, J. Jastrzębski, P. Lubiński, F. J. Hartmann, R. Schmidt, T. von Egidy, and B. Kłos, Phys. Rev. Lett. **87**, 082501 (2001).
[45] J. Jastrzębski, A. Trzcińska, P. Lubiński, B. Kłos, F. J. Hartmann, T. von Egidy, and S. Wycech, Int. J. Mod. Phys. E **13**, 343 (2004).
[46] Y. Ren and Z. Ren, Phys. Rev. C **85**, 044608 (2012).
[47] V. Yu. Denisov, O. I. Davidovskaya, and I. Yu. Sedykh, Phys. Rev. C **92**, 014602 (2015).
[48] S. Cwiok, J. Dudek, W. Nazarewicz, J. Skalski, and T. Werner, Comput. Phys. Commun. **46**, 379 (1987).
[49] M. Wang, G. Audi, A. H. Wapstra, F. G. Kondev, M. MacCormick, X. Xu, and B. Pfeiffer, Chin. Phys. C **36**, 1603 (2012).
[50] J. Suhonen and O. Civitarese, Phys. Lett. B **725**, 153 (2013).
[51] J. Suhonen and O. Civitarese, Nucl. Phys. A **924**, 1 (2014).
[52] T. Marketin, L. Huther, and G. Martínez-Pinedo, Phys. Rev. C **93**, 025805 (2016).
[53] I. N. Borzov, Phys. Rev. C **67**, 025802 (2003).
[54] I. N. Borzov, J. J. Cuenca-García, K. Langanke, G. Martínez-Pinedo, and F. Montes, Nucl. Phys. A **814**, 159 (2008).
[55] F. F. Deppisch and J. Suhonen, Phys. Rev. C **94**, 055501 (2016).
[56] A. P. Severyukhin, V. V. Voronov, I. N. Borzov, N. N. Arsenyev, and N. Van Giai, Phys. Rev. C **90**, 044320 (2014).
[57] Y. F. Niu, Z. M. Niu, G. Colo, and E. Vigezzi, Phys. Rev. Lett. **114**, 142501 (2015).
[58] I. Angeli, At. Data Nucl. Data Tables **87**, 185 (2004).
[59] P. E. Hodgson and E. Běták, Phys. Rep. **374**, 1 (2003).
[60] T. L. Stewart, M. W. Kermode, D. J. Beachey, N. Rowley, I. S. Grant, and A. T. Kruppa, Phys. Rev. Lett. **77**, 36 (1996).